Metallothermic Combustion Reaction on Synthesis of Titanium Boride-Spinel Composites

Chun-Liang Yeh, Fu-You Zheng
Department of Aerospace and Systems Engineering, Feng Chia University
Taichung, Taiwan

1 Introduction

TiB_2 has been one of the most studied ultra-high temperature ceramics (UHTCs) due to its unique properties, including a high melting point (3225 $^{\circ}$C), high hardness (33 MPa), high Young's modulus (530 MPa), excellent wear and oxidation resistance, thermal shock resistance, chemical inertness, and good electric conductivity [1]. Combination of these properties makes TiB_2 an ideal candidate for use in ballistic armors, crucibles, metal evaporation boats, cutting tools, wear resistance parts, and cathodes for alumina smelting [1]. Many ceramic phases, such as Al_2O_3, SiC, B_4C, and $MgAl_2O_4$, have been considered as the reinforcement to improve fracture toughness, oxidation resistance, heat resistance, and mechanical strength of the TiB_2-based composites [1-3]. Magnesium aluminate spinel, $MgAl_2O_4$, as an additive has been rarely studied, possibly because the fabrication of $MgAl_2O_4$ via either the direct solid-state reaction of oxides or wet chemical methods requires multiple steps that are complicated and time-consuming [4,5]. However, $MgAl_2O_4$ is an attractive component due to its high melting point, chemical inertness, high hardness, corrosion resistance, high mechanical strength, and low cost [4].
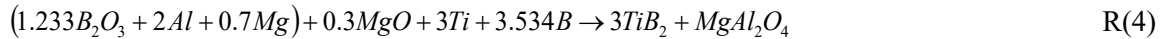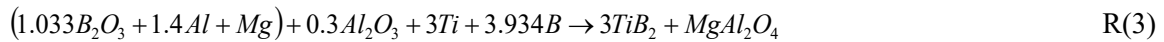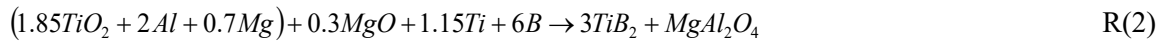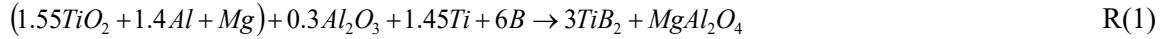
Among various fabrication routes for preparing multiphasic ceramics, metallothermic reduction reactions (i.e., thermite reactions) combined with combustion synthesis have been recognized as a promising technique for in situ formation of $MgAl_2O_4$–containing composites. Combustion synthesis in the mode of self-propagating high-temperature synthesis (SHS), which is based on strongly exothermic reactions, has merits of low energy consumption, short reaction time, simple operation and equipment, high-purity products, and in situ formation of composite components [6]. Moreover, aluminothermic and magnesiothermic reduction reactions have Al_2O_3 and MgO as their respective by-products, both of which are precursors for the formation of $MgAl_2O_4$. Consequently, Omran et al. [7] applied the reduction-based SHS technique to produce $MgAl_2O_4$–W–W_2B composites through magnesiothermic reduction of WO_3 and B_2O_3 in the presence of Al_2O_3. Zaki et al. [8] synthesized $MoSi_2$– and Mo_5Si_3–$MgAl_2O_4$ composites by SHS with a reducing stage from raw materials consisting of MoO_3, SiO_2, and Al as aluminothermic reagents and MgO as a precursor.

This study represents the first attempt to prepare TiB_2–$MgAl_2O_4$ in situ composites from the SHS powder metallurgy simultaneously involving aluminothermic and magnesiothermic reduction of TiO_2 or B_2O_3. Only a small amount of Al_2O_3 or MgO was included in the reactive mixture to serve as the combustion moderator and part of the precursors for the formation of $MgAl_2O_4$. Four SHS reaction

systems formulated with different metallothermic reagents and combustion diluents were investigated. In this work, combustion exothermicity and combustion wave kinetics of the SHS process, as well as compositions and microstructures of the final products were explored.

2   Experimental Methods of Approach

The starting materials adopted by this study included TiO$_2$ (Acros Organics, 99.5%), B$_2$O$_3$ (Acros Organics, 99%), Al$_2$O$_3$ (Alfa Aesar, 99%), MgO (Acros Organics, 99.5%), Al (Showa Chemical Co., < 45 μm, 99.9%), Mg (Alfa Aesar, < 45 μm, 99.8%), Ti (Alfa Aesar, < 45 μm, 99.8%), and amorphous boron (Noah Technologies, < 1 μm, 93.5%). Four SHS reactions were formulated for the synthesis of 3TiB$_2$–MgAl$_2$O$_4$ composites. Two metallothermic reagents (i.e., thermites) were considered; one is composed of TiO$_2$, Al, and Mg, as shown in R(1) and R(2), and the other comprises B$_2$O$_3$, Al, and Mg, as in R(3) and R(4). Due to strong exothermicity of combustion, Al$_2$O$_3$ with an amount of 0.3 mol. was included in R(1) and R(3) as the combustion moderator (or combustion diluent) in order to attain stable propagation of the combustion wave. The pre-added Al$_2$O$_3$ also acted as part of the precursor for the synthesis of MgAl$_2$O$_3$. Likewise, an equal amount of MgO was adopted by R(2) and R(4) and MgO played the same role as Al$_2$O$_3$ in R(1) and R(3).

$$\left(1.55TiO_2 + 1.4Al + Mg\right) + 0.3Al_2O_3 + 1.45Ti + 6B \rightarrow 3TiB_2 + MgAl_2O_4 \qquad \text{R(1)}$$

$$\left(1.85TiO_2 + 2Al + 0.7Mg\right) + 0.3MgO + 1.15Ti + 6B \rightarrow 3TiB_2 + MgAl_2O_4 \qquad \text{R(2)}$$

$$\left(1.033B_2O_3 + 1.4Al + Mg\right) + 0.3Al_2O_3 + 3Ti + 3.934B \rightarrow 3TiB_2 + MgAl_2O_4 \qquad \text{R(3)}$$

$$\left(1.233B_2O_3 + 2Al + 0.7Mg\right) + 0.3MgO + 3Ti + 3.534B \rightarrow 3TiB_2 + MgAl_2O_4 \qquad \text{R(4)}$$

Combustion exothermicity of the above four reactions was evaluated by calculating their adiabatic combustion temperatures (T_{ad}) from the following energy balance equation [9] with thermochemical data taken from [10].

$$\Delta H_r + \int_{298}^{T_{ad}} \sum n_j\, c_p\left(P_j\right) dT + \sum_{298-T_{ad}} n_j\, L\left(P_j\right) = 0$$

where ΔH_r is the reaction enthalpy at 298 K, n_j is the stoichiometric coefficient, c_p and L are the heat capacity and latent heat, and P_j refers to the product component.

The SHS experiments were conducted in a windowed combustion chamber under argon of 0.25 MPa. Reactant powders were well mixed in a ball mill and uniaxially compressed into cylindrical test specimens with a diameter of 7 mm, a height of 12 mm, and a relative density of 55%. The ignition of sample compacts was achieved by an electrically heated tungsten coil. The combustion wave propagation velocity (V_f) was determined by the time derivative of the flame-front trajectory constructed from the recorded series of combustion images. The combustion temperature was measured by the R-type (Pt/Pt-13%Rh) bare-wire thermocouple with a bead size of 125 μm. Phase compositions of the products were identified by an X-ray diffractometer (XRD, Bruker D2 Phaser). Microstructures and constituent elements of the products were examined by the scanning electron microscopy (SEM, Hitachi, S3000H) and energy dispersive spectroscopy (EDS). Details of the experimental methods were reported elsewhere [11].

3   Results and Discussion

Figure 1 presents the calculated ΔH_r and T_{ad} of reactions R(1)-R(4) and shows that R(4) has the highest values while R(1) has the lowest ones. Both ΔH_r and T_{ad} increases from R(1) to R(4). Specifically, the values of T_{ad} are 2530 K, 2595 K, 2783 K, 2897 K for R(1), R(2), R(3), and R(4), respectively. A

comparison between R(1) and R(2) revealed that the combustion moderator Al_2O_3 appeared to impose a stronger dilution effect on combustion than MgO, which led to a lower T_{ad} for R(1) than R(2). Similar results were observed in R(3) and R(4). These findings could also be explained by the fact that metallothemic reduction of TiO_2 or B_2O_3 by Al is more exothermic than that by Mg [10].

On the other hand, because the B_2O_3-based thermite is more energetic than the one using TiO_2 [10], R(3) has a higher T_{ad} than R(1). Similarly, R(4) has a higher T_{ad} than R(2). According to the calculated T_{ad}, it is realized that the thermite oxidants (i.e., B_2O_3 versus TiO_2) have a more pronounced influence on combustion exothermicity than the diluent oxides (i.e., Al_2O_3 versus MgO).
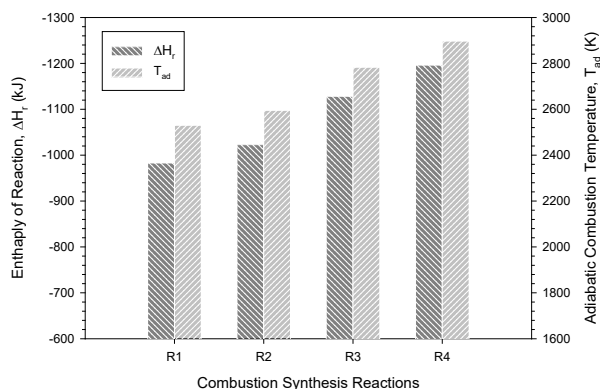

Figure 1: Enthalpies of reaction (ΔH_r) and adiabatic combustion temperatures (T_{ad}) of SHS reactions.

Two series of the SHS processes recorded from reactions R(1) and R(3) are illustrated in Figure 2(a) and (b), respectively. It is apparent that upon ignition, the reaction was initiated and characterized by a self-sustaining combustion wave. More intense combustion accompanied with a faster combustion wave was observed in Figure 2(b), when compared with that in Figure 2(a). Combustion luminosity and flame spreading speed reflected the degree of reaction exothermicity. As mentioned above, B_2O_3/Al/Mg-based R(3) is more energetic than TiO_2/Al/Mg-based R(1). Similar combustion behavior was also noticed in R(2) and R(4).
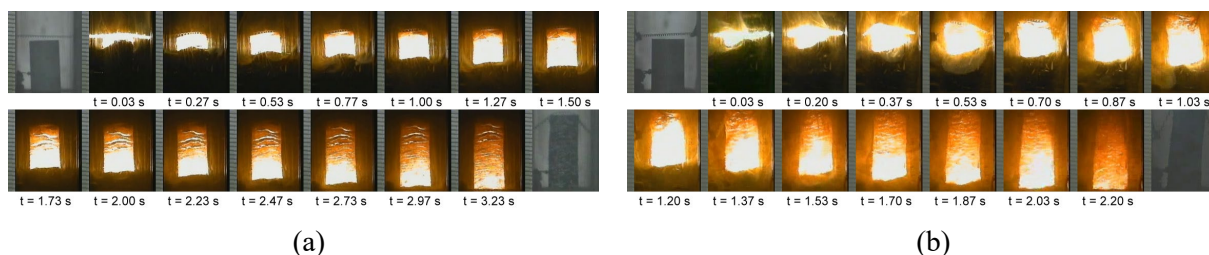

(a)	(b)

Figure 2: Time sequences of recorded SHS images illustrating self-sustaining combustion wave of (a) R(1) and (b) R(3).

Figure 3 depicts typical combustion temperature profiles measured from four different reactions. All profiles exhibit a steep thermal gradient followed by a rapid descent, which is inherent in the SHS reaction that features a rapid combustion wave and a thin reaction zone. The peak value is considered as the combustion front temperature (T_c). When compared with pinnacles in the contours of R(1) and R(2), sharper peaks were detected in the profiles of R(3) and R(4) This implied a faster combustion wave in R(3) and R(4). As shown in Figure 3, the values of T_c from R(1) to R(4) in ascending order are 1348 °C, 1445 °C, 1660 °C, and 1736 °C. It should be noted that the measured combustion front temperatures are in agreement with the calculated reaction exothermicity.

Figure 4 plots the measured combustion wave propagation velocities (V_f) and temperatures (T_c) of four reactions. The rising trend of V_f from R(1) to R(4) is consistent with that of T_c. This can be explained

by the fact that combustion wave propagation is essentially governed by layer-by-layer heat transfer from the thin combustion zone to unreacted region, and therefore, is subject to the reaction front temperature. As presented in Figure 4, the average combustion velocities are 3.9, 4.7, 5.1, and 5.7 mm/s for R(1), R(2), R(3), and R(4), respectively. It is worth noting that the measured combustion temperature not only justified the reaction exothermic analysis, but also confirmed the temperature dependence of combustion wave velocity.
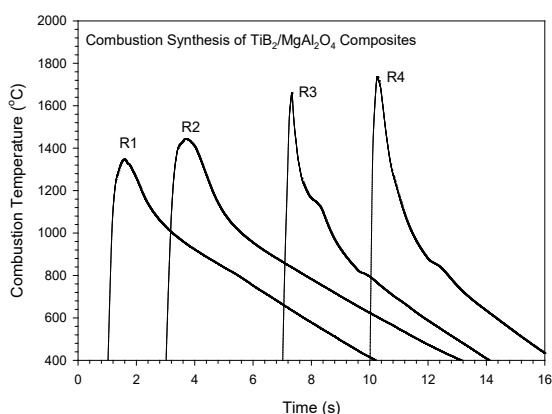
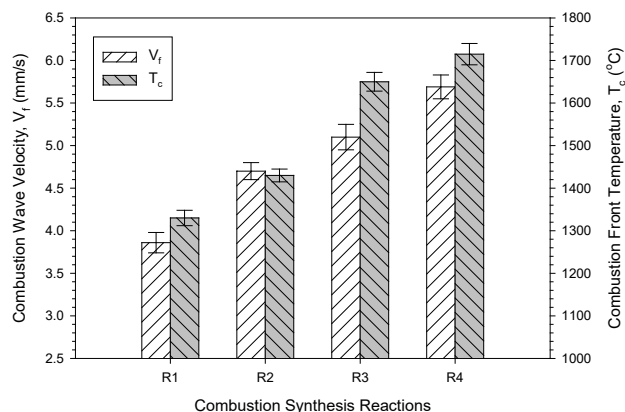| Figure 3: Typical combustion temperature profiles of R(1), R(2), R(3), and R(4). | Figure 4: Measured combustion wave velocity (V_f) and combustion front temperature (T_c). |

The XRD spectra of the final products synthesized from R(1) and R(2) are shown in Figure 5(a) and (b), respectively. Both indicated the formation of TiB_2 and $MgAl_2O_4$ along with two minor phases, magnesium titanate ($MgTiO_3$) and MgO. It is believed that $MgAl_2O_4$ was synthesized through a combination reaction between Al_2O_3 and MgO. R(1) and R(2) were formulated with the same thermite reagents of TiO_2, Al, and Mg, but diluted by different metal oxides. That is, Al_2O_3 was partly pre-added and partly thermite-produced, while MgO was all generated from the reduction of TiO_2 by Mg in R(1). In contrast, the required Al_2O_3 in R(2) was entirely produced from the reduction of TiO_2 by Al, but MgO was supplied in part from prior addition and in part from the reduction of TiO_2 by Mg. For both R(1) and R(2), TiB_2 was synthesized from the reaction of elemental boron with reduced and metallic Ti. Traces of MgO suggested an incomplete reaction due probably to the relatively low reaction temperatures of R(1) and R(2). The presence of $MgTiO_3$ in the final products of R(1) and R(2) could be attributed to the reaction of MgO with the thermite oxidant TiO_2.

Figure 6(a) and (b) exhibits the XRD patterns of the synthesized composites from R(3) and R(4), respectively. In addition to TiB_2 and $MgAl_2O_4$, a small amount of $MgTiO_3$ was identified. The formation of $MgAl_2O_4$ from a combination reaction between Al_2O_3 and MgO was proved. Both Al_2O_3 and MgO can be totally or partially produced from the reduction of B_2O_3 by Al and Mg. For R(3) and R(4) containing B_2O_3/Al/Mg-based thermite, TiB_2 was produced from the reaction of metallic Ti with reduced and elemental boron. Moreover, the formation of $MgTiO_3$ in R(3) and R(4) might involve some interaction of Ti with B_2O_3 to form TiO_2 which further reacted with MgO. Unlike that in R(1) and R(2), MgO was no longer detected in the final products of R(3) and R(4).

The microstrcture of fracture surface of the synthesized product of R(1) shows several large and solidified $MgAl_2O_4$ aggregates of 5–15 μm surrounded by fine-grain TiB_2 crystals with a particle size of about 1–2 μm. For the final product of B_2O_3/Al/Mg-based R(4), the microstructure and atomic ratios of constituent elements are presented in Figure 7. As can be seen, $MgAl_2O_4$ was formed as large densified aggregates of around 20 μm and TiB_2 crystals were in a short-rod form with a length of 2–4 μm or in a shape of fine grains of 1–2 μm. Based on the EDS analysis, the atomic ratio of the selected

area in an aggregate is Mg:Al:O = 15.1:30.6:54.3 that is reasonably close to $MgAl_2O_4$. Short-rod crystals have a composition of Ti:B = 34.3:65.7, which certainly is TiB_2.
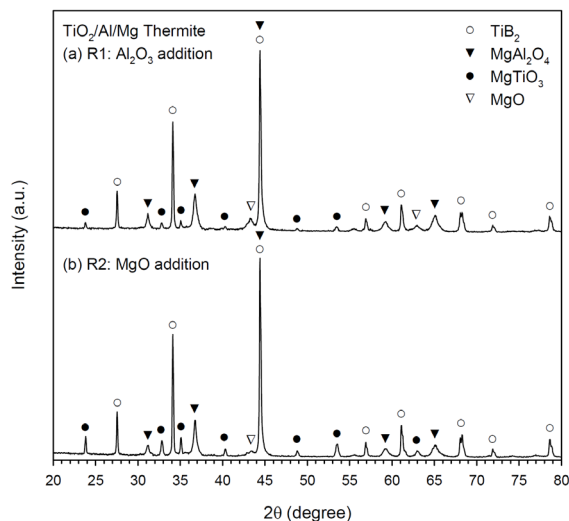

Figure 5: XRD patterns of final products of (a) R(1) and (b) R(2).

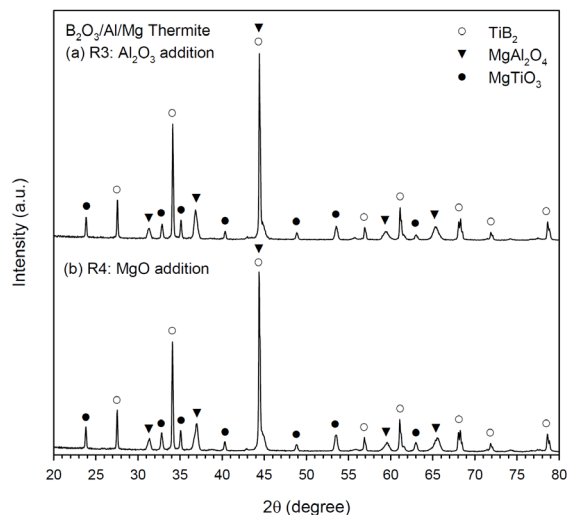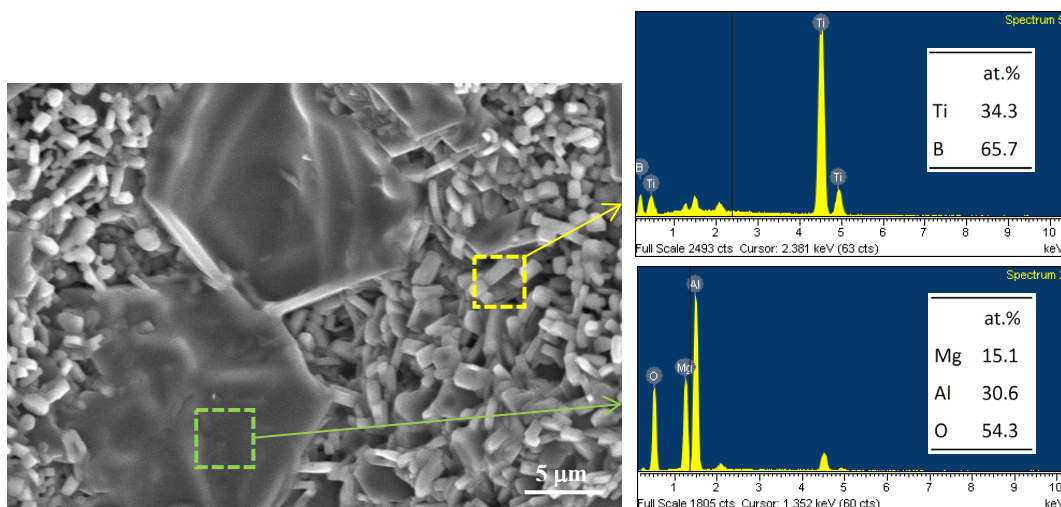Figure 6: XRD patterns of final products of (a) R(3) and (b) R(4).

Figure 7: SEM micrograph and EDS spectra of $TiB_2/MgAl_2O_4$ composite synthesized from R(4).

4   Conclusion

In situ formation of $3TiB_2$–$MgAl_2O_4$ composites was conducted by combustion synthesis combined with metallothermic reduction reactions involving Al and Mg as dual reductants. Thermite reagents with different oxidants were considered; one utilized TiO_2 and the other B_2O_3. The reactant mixtures also contained elemental Ti and boron. The overall synthesis reaction was exothermic enough to proceed in the SHS mode. The analysis of combustion exothermicity indicated that the SHS reaction containing B_2O_3/Al/Mg-based thermites was more energetic than that adopting TiO_2 as the oxidant. Prior addition of Al_2O_3 had a stronger dilution effect on combustion than that of MgO. Depending on

different thermites and diluents, the measured combustion front temperatures ranged from 1320 to 1720 °C, and combustion wave velocity from 3.9 to 5.7 mm/s. The temperature dependence of combustion wave velocity was justified. The XRD analysis confirmed in situ formation of TiB$_2$ and MgAl$_2$O$_4$. A small amount of MgTiO$_3$ was found as the impurity. It is believed that MgAl$_2$O$_4$ was synthesized through a combination reaction between Al$_2$O$_3$ and MgO, both of which can be totally or partially produced from the metallothermic reduction of B$_2$O$_3$ or TiO$_2$. The microstructure of the synthesized composite exhibited that MgAl$_2$O$_4$ was surrounded by closely-packed TiB$_2$ grains. MgAl$_2$O$_4$ was formed as densified aggregates with a size of 5-20 μm. TiB$_2$ crystals were produced in a shape of short rods of 2–4 μm and fine grains of 1–2 μm. An energy-saving and efficient fabrication route for the formation MgAl$_2$O$_4$-containing composites was demonstrated by this study.

Acknowledgments

References

[1] Munro RG. (2000). Material properties of titanium diboride. J. Res. Natl. Inst. Stand. Technol. 105: 709-720.

[2] Yu. Popov A. Sivak AA. Yu. Borodianska H. Shabalin IL. (2015) High toughness TiB$_2$–Al$_2$O$_3$ composite ceramics produced by reactive hot pressing with fusible components. Adv. Appl. Ceram. 114: 178-182.

[3] Radishevskaya N. Lepakova O. Karakchieva N. Nazarova A. Afanasiev N. Godymchuk A. Gusev A. (2017) Self-propagating high temperature synthesis of TiB$_2$–MgAl$_2$O$_4$ composites. Metals 7: 295.

[4] Ganesh I. (2013). A review on magnesium aluminate (MgAl$_2$O$_4$) spinel: synthesis, processing and applications. Int. Mater. Rev. 58: 63-112.

[5] Yuan L. Tian C. Yan X. He X. Liu Z. Wen T. Jin E. Yu J. (2021). Preparation of porous MgAl$_2$O$_4$ ceramics by a novel pectin gel-casting process. J. Aust. Ceram. Soc. 57: 1049-1055.

[6] Levashov EA. Mukasyan AS. Rogachev AS. Shtansky DV. (2017). Self-propagating high-temperature synthesis of advanced materials and coatings. Int. Mater. Rev. 62: 203-239.

[7] Omran JG. Afarani MS. Sharifitabar M. (2018). Fast synthesis of MgAl$_2$O$_4$–W and MgAl$_2$O$_4$–W–W$_2$B composite powders by self-propagating high-temperature synthesis reactions. Ceram. Int. 44: 6508-6513.

[8] Zaki ZI. Mostafa NY. Rashad MM. (2012). High pressure synthesis of magnesium aluminate composites with MoSi$_2$ and Mo$_5$Si$_3$ in a self-sustaining manner. Ceram. Int. 38: 5231-5237.

[9] Liang YH. Wang HY. Yang YF. Zhao RY. Jiang QC. (2008). Effect of Cu content on the reaction behaviors of self-propagating high-temperature synthesis in Cu-Ti-B$_4$C system. J. Alloys Compd. 462: 113–118.

[10] Binnewies M. Milke E. (2002). Thermochemical Data of Elements and Compounds, Wiley-VCH Verlag GmbH: Weinheim, Germany (ISBN 9783527305247).

[11] Yeh CL. Lin JZ. (2013). Combustion synthesis of Cr-Al and Cr-Si intermetallics with Al$_2$O$_3$ additions from Cr$_2$O$_3$-Al and Cr$_2$O$_3$-Al-Si reaction systems. Intermetallics 33: 126–133.